Eur. Phys. J. C 316, 337–347 (2000)
Digital Object Identifier (DOI) 10.1007/s100520000369

THE EUROPEAN PHYSICAL JOURNAL C

© Società Italiana di Fisica
Springer-Verlag 2000

Structure function of the nucleus in the perturbative QCD with $N_c \to \infty$ (BFKL pomeron fan diagrams)

M. Braun

Department of High Energy Physics, University of St. Petersburg, 198904 St. Petersburg, Russia

Received: 26 January 2000 / Published online: 8 June 2000 – © Springer-Verlag 2000

Abstract. The equation for the sum of BFKL pomeron fan diagrams is rederived by a direct summation and solved numerically for rapidities $y \leq 50$. At high rapidities, $y > 20$, the resulting cross-sections for the scattering of a longitudinally polarized $q\bar{q}$ pair on the nucleus cease to depend on its transverse dimension and tend to a constant limit of $0.1768R_A^2$, which corresponds to scattering of a color dipole on a black disk. Thus the unitarity is restored and the singularity in the j plane is reduced to a simple pole at $j = 1$. The nuclear structure function at small x behaves as $Q^2 \ln(1/x)$. The gluon density found has a soliton-like form in the $\log k$ space: its form is close to Gaussian, independent of rapidity, the center moving towards higher $\log k$ with a nearly constant velocity as the rapidity increases.

1 Introduction

In the framework of the color dipole model of Mueller [1, 2] it follows that in the high-color limit $N_c \to \infty$ the scattering on a heavy nucleus is exactly described by the sum of fan diagrams constructed of BFKL pomerons, each of them splitting into two [3]. This sum seems to be unitary by itself. It is important that no splitting into three or more pomerons, as introduced in [4], occurs, although formally they give contributions of the same order. Because of this fact, once the splitting vertex is known, the construction of the amplitude for the interaction with the nucleus becomes straightforward, reducing to summing BFKL pomeron fan diagrams. This procedure has been well known since the times of the old Regge–Gribov theory [5].

In the perturbative QCD a pioneering step was taken also many years ago by Gribov, Levin and Ryskin, who summed fan diagrams in the double log approximation and wrote their well-known non-linear GLR equation [6]. In the framework of the BFKL dynamics, the necessary tool for constructing fan diagrams is the corresponding triple pomeron vertex, which was found in the color dipole approach for $N_c \to \infty$ by Mueller and Patel [2] and in the s-channel unitarity approach for any number of colors by Bartels and Wuesthoff [7]. The equivalence of both results was shown in [8].

The equation for the sum of BFKL fan diagrams with this splitting vertex was written by Balitsky [9] in his original operator expansion formalism and by Kovchegov [10] in the color dipole framework (with a somewhat unconventional form of the coupling to the target). Its perturbative solution in the region of small non-linearity (outside the saturation region) was studied in [11]. Asymptotic estimates of the solution were presented in [12].

In the present paper we first rederive the BFKL fan diagram equation by direct summation using the standard form of the pomeron–target coupling. It has the form of a simple (and elegant) evolution equation in rapidity y for a wave function $\phi(y, q)$ in the momentum space:

$$\frac{\partial \phi(y,q)}{\partial y} = -H\phi(y,q) - \phi^2(y,q), \qquad (1)$$

where H is the BFKL Hamiltonian for the so-called semi-amputated function (a similar form was also obtained in [11]).

In spite of its tantalizing simplicity, (1) does not seem to allow for an analytical treatment except by perturbative methods, not valid in the most interesting region of strong non-linear effects, or by qualitative asymptotic estimates. The bulk of this paper is correspondingly devoted to its numerical analysis. We numerically study the evolution of the wave function in the rapidity, starting from an appropriately chosen initial function. The results are then used to find the structure function of the nucleus at small $x = \mathrm{e}^{-y}$ and various virtualities Q^2. Our results show that for a heavy nucleus the longitudinal part of the structure function saturates at $x \to 0$ to a universal function $F_{2\mathrm{L}}^{(\mathrm{as})}(Q^2)$, independent of the nucleus atomic number but strongly dependent on Q^2 in the whole range of $Q^2 \leq 10^5\,(\mathrm{GeV}/c)^2$ explored. In fact $F_{2\mathrm{L}}^{(\mathrm{as})}(Q^2)$ is just proportional to Q^2. This reflects the behavior of the scattering cross-section of a longitudinally polarized $q\bar{q}$ pair on the nucleus: at very small x it becomes independent of both the pair size and x. The latter property indicates that unitarity is restored and the leading singularity in the complex momentum j is reduced to a simple pole at $j = 1$. Note that the limiting cross-section is in accordance with the picture in which the longitudinally polarized photon

with a certain probability splits into color dipoles, which then scatter on the nucleus as on a black disk. For the leading transverse part of the structure function this probability result turns out to be infinite. Due to this fact both the cross-section and the structure function continue to grow at $x \to 0$ approximately as $\ln(1/x)$. These results are in agreement with predictions made in [11,12].

As to the gluon density, we have found it to have a Gaussian shape as a function of $\xi = \ln k$ with a center at $\xi_0 \propto y$. So with the growth of rapidity it propagates towards higher momenta, practically preserving its form, very much like a soliton wave. Obvious limitations on computing time and memory allow one to follow its movement up to momenta not higher than of the order of $10^{10}\,\mathrm{GeV}/c$. However, we expect that this behavior persists in the model until arbitrary high values of momenta. As a result, at any fixed value of k the density eventually goes to zero as $y \to \infty$. In this sense we have the maximal saturation of the density possible.

The paper is organized as follows. In Sect. 2 we present a derivation of the BFKL fan diagram equation by a direct summation. Sect. 3 is devoted to the numerical solution of (1). In Sect. 4 the nuclear structure function and gluon density are calculated. Section 5 contains our conclusions. In the Appendix we compare our BFKL fan diagram equation with the Kovchegov one [10].

2 Fan diagram equation for the BFKL pomerons

We start with a single scattering contribution to the forward ampitude for the interaction of the projectile particle with a nucleus.

In the BFKL framework, at fixed impact parameter b, it has a well-known form:

$$\mathcal{A}_1(y,b) = \mathrm{i}sg^4 AT(b) \int \mathrm{d}^2r\mathrm{d}^2r'\rho(r)G(y,r,r')\rho_N(r'). \quad (2)$$

Here ρ and ρ_N are the color densities of the projectile and the target nucleon respectively. The function G is the forward BFKL Green function [13]:

$$G(y,r,r') = \frac{rr'}{32\pi^2} \sum_{n=-\infty}^{+\infty} \mathrm{e}^{\mathrm{i}n(\phi-\phi')} \times \int_{-\infty}^{\infty} \frac{\mathrm{d}\nu \mathrm{e}^{y\omega(\nu)}}{[\nu^2+(n-1)^2/4][\nu^2+(n+1)^2/4]} \times (r/r')^{-2\mathrm{i}\nu}, \quad (3)$$

where ϕ and ϕ' are the azimuthal angles and

$$\omega(\nu) = 2(\alpha_s N/2\pi)(\psi(1) - \mathrm{Re}\psi(1/2+\mathrm{i}\nu)) \quad (4)$$

are the BFKL levels. Due to the azimuthal symmetry of the projectile color density one may retain only the term with zero orbital momenta $n = 0$ in (3). Separating the projectile part, the single scattering term may be written in the form

$$\mathcal{A}_1(y,b) = 2\mathrm{i}s \int \mathrm{d}^2r\rho(r)\Phi_1(y,b,r), \quad (5)$$

where

$$\Phi_1(y,b,r) = \frac{1}{2}g^4 AT(b) \int \mathrm{d}^2r' G(y,r,r')\rho_N(r'). \quad (6)$$

The double scattering contribution has been calculated in [14]. In the limit $N_c >> 1$ one finds

$$\mathcal{A}_2(y,b) = -\mathrm{i}s\frac{g^2N_c}{4\pi^3} \int \mathrm{d}^2r\rho(r) \int_0^y \mathrm{d}y_2 \times \int \prod_{i=1}^{3} \mathrm{d}^2r_i\delta^2(r_1+r_2+r_3) \frac{r_1^2\nabla_1^4}{r_2^2r_3^2} G(y-y_2,r,r_1) \times \Phi_1(y_2,b,r_2)\Phi_1(y_2,b,-r_3). \quad (7)$$

Representing $\mathcal{A}_2$ in terms of Φ_2 similarly to (5) we find

$$\Phi_2(y,b,r) = -\frac{g^2N_c}{8\pi^3} \int_0^y \mathrm{d}y_2 \int \prod_{i=1}^{3} \mathrm{d}^2r_i\delta^2(r_1+r_2+r_3) \times \frac{r_1^2\nabla_1^4}{r_2^2r_3^2} G(y-y_2,r,r_1)\Phi_1(y_2,b,r_2)\Phi_1(y_2,b,-r_3). \quad (8)$$

The whole set of fan diagrams will evidently be summed by the equation which is graphically illustrated in Fig. 1:

$$\Phi(y,b,r) = \Phi_1(y,b,r) - \frac{g^2N_c}{8\pi^3} \int_0^y \mathrm{d}y_2 \times \int \prod_{i=1}^{3} \mathrm{d}^2r_i\delta^2(r_1+r_2+r_3) \frac{r_1^2\nabla_1^4}{r_2^2r_3^2} G(y-y_2,r,r_1) \times \Phi(y_2,b,r_2)\Phi(y_2,b,-r_3). \quad (9)$$

The impact parameter b appears here only as a parameter and the dependence on it will be implicit in the following. In terms of Φ the total forward scattering amplitude on the nucleus will be given at fixed b by

$$\mathcal{A}(y,b) = 2\mathrm{i}s \int \mathrm{d}^2r\rho(r)\Phi(y,b,r). \quad (10)$$

One can rewrite (9) as an evolution equation in y. To this end we represent Φ as an integral over the ν's similar to (3):

$$\Phi(y,r) = \int \mathrm{d}\nu r^{1-2\mathrm{i}\nu}\Phi(y,\nu).$$

Then from (9) we find

$$\Phi(y,\nu) = \frac{g^4}{64\pi^2(\nu^2+1/4)^2}\mathrm{e}^{\omega(\nu)y} \int \mathrm{d}^2r' r'^{1+2\mathrm{i}\nu}\rho(r')AT(b) - \frac{g^2N_c}{32\pi^5(\nu^2+1/4)^2}\mathrm{e}^{\omega(\nu)y} \int_0^y \mathrm{d}y_2\mathrm{e}^{-\omega(\nu)y_2} \times \int \prod_{i=1}^{3} \mathrm{d}^2r_i\delta^2(r_1+r_2+r_3) \times \frac{r_1^2\nabla_1^4}{r_2^2r_3^2} r_1^{1-2\mathrm{i}\nu}\Phi(y_2,r_2)\Phi(y_2,-r_3). \quad (11)$$

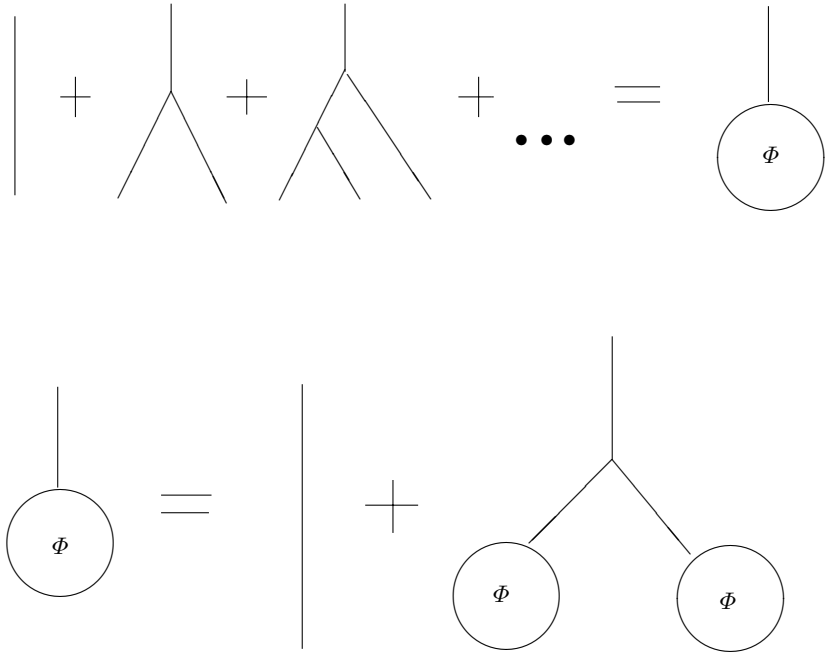

Fig. 1. The equation summing fan diagrams. Lines represent pomerons

Multiplying both parts by $\mathrm{e}^{-\omega(\nu)y}$ and taking the derivative in y we obtain

$$\left(\frac{\partial}{\partial y} - \omega(\nu)\right)\Phi(y,\nu) = -\frac{g^2 N_c}{32\pi^5(\nu^2+1/4)^2} \times \int\prod_{i=1}^{3}\mathrm{d}^2 r_i \delta^2(r_1+r_2+r_3) \times \frac{r_1^2\nabla_1^4}{r_2^2 r_3^2} r_1^{1-2\mathrm{i}\nu}\Phi(y,r_2)\Phi(y,-r_3). \quad (12)$$

Returning to the r space we take into account that

$$\omega(\nu) r^{1-2\mathrm{i}\nu} = -\hat{H} r^{1-2\mathrm{i}\nu}, \quad (13)$$

where $\hat{H}$ is the BFKL Hamiltonian [13]. Then (12) transforms into

$$\left(\frac{\partial}{\partial y} + \hat{H}\right)\Phi(y,r) = -\frac{g^2 N_c}{8\pi^3}\int\prod_{i=1}^{3}\mathrm{d}^2 r_i \delta^2(r_1+r_2+r_3) \times \frac{r_1^2\nabla_1^4}{r_2^2 r_3^2} G(0,r,r_1)\Phi(y,r_2)\Phi(y,-r_3). \quad (14)$$

Using

$$\frac{r_1^2\nabla_1^4}{r^2}G(0,r,r_1) = \frac{1}{2\pi^2 r r_1}\sum_{n=-\infty}^{+\infty}\mathrm{e}^{\mathrm{i}n(\phi-\phi_1)}\int_{-\infty}^{\infty}\mathrm{d}\nu (r/r_1)^{-2\mathrm{i}\nu} = \delta^2(r-r_1), \quad (15)$$

we simplify (14) to the form

$$\left(\frac{\partial}{\partial y} + \hat{H}\right)\Phi(y,r) = -\frac{g^2 N_c}{8\pi^3}\int\prod_{i=2}^{3}\mathrm{d}^2 r_i \delta^2(r+r_2+r_3) \times \frac{r^2}{r_2^2 r_3^2}\Phi(y,r_2)\Phi(y,-r_3). \quad (16)$$

The initial condition is determined from (9) to be

$$\Phi(y,r)_{y=0} = \Phi_0(r) \quad (17)$$

with

$$\Phi_0(r) = \frac{1}{2}g^4 A T(b)\int \mathrm{d}^2 r' G(0,r,r')\rho(r'). \quad (18)$$

Except for the initial condition and different variables, (16) coincides with the one constructed by Kovchegov in the color dipole approach in [10] (see the Appendix).

Now we go to the function

$$\phi(y,r) = \frac{1}{r^2}\Phi(y,r) \quad (19)$$

and pass to the momentum space. For $\phi(y,q)$ (16) reads

$$\left(\frac{\partial}{\partial y} + \frac{1}{r^2}\hat{H}r^2\right)\phi(y,q) = -\frac{g^2 N_c}{8\pi^3}\phi(y,q)\phi(y,q), \quad (20)$$

where we have used that $\phi(y,q)$ in fact depends only on $|q|$, which follows from the initial condition

$$\phi_0(y,q)_{y=0} = \int\frac{\mathrm{d}^2 r}{r^2}\mathrm{e}^{-\mathrm{i}qr}\Phi_0(r), \quad (21)$$

with Φ_0 given by (18) and depending only on $|r|$ due to the azimuthal symmetry.

The Hamiltonian $r^{-2}\hat{H}r^2$ which appears on the left-hand side is the standard forward Hamiltonian for the semi-amputated functions

$$\frac{1}{r^2}\hat{H}r^2 = H = \frac{g^2N_c}{4\pi^2}[\ln q^2 + \ln r^2 - 2(\ln 2 + \psi(1))]. \quad (22)$$

Indeed the eigenfunctions of $\hat{H}$, $\Phi_{n,\nu}(r) = r^{1-2i\nu}e^{in\phi}$, go over into the eigenfunctions of H after division by r^2.

This brings us to nearly the final form of our equation

$$\left(\frac{\partial}{\partial y} + H\right)\phi(y,q) = -\frac{g^2N_c}{8\pi^3}\phi^2(y,q). \quad (23)$$

It remains only to appropriately rescale H, ϕ and y to obtain the BFKL fan diagram equation in the final form (1). We introduce

$$H = \frac{g^2N_c}{4\pi^2}\tilde{H}, \quad \tilde{y} = \frac{g^2N_c}{4\pi^2}y, \quad \text{and} \quad \phi(\tilde{y},q) = 2\pi\tilde{\phi}(\tilde{y},q), \quad (24)$$

where

$$\tilde{H} = \ln r^2 + \ln q^2 - 2(\ln 2 + \psi(1)). \quad (25)$$

The equation for $\tilde{\phi}$ takes the form (1)

$$\left(\frac{\partial}{d\tilde{y}} + \tilde{H}_0\right)\tilde{\phi}(\tilde{y},q) = -\tilde{\phi}^2(\tilde{y},q) \quad (26)$$

with the initial condition

$$\tilde{\phi}(\tilde{y},q)_{\tilde{y}=0} = \frac{g^4AT(b)}{4\pi}\int d^2r d^2r_1 \frac{1}{r^2}e^{iqr}G(0,r,r_1)\rho_N(r_1). \quad (27)$$

3 Numerical solution of the BFKL fan diagram equation

To solve numerically (26) we first transform the BFKL Hamiltonian H to more convenient variables. In the momentum space one can write the action of H on a function $\phi(q)$ as

$$H\phi(q) = -2\int_0^\infty k dk \times \left[\frac{\phi(k) - (q^2/k^2)\phi(q)}{|q^2 - k^2|} + \frac{q^2}{k^2}\frac{\phi(q)}{\sqrt{4k^4 + q^4}}\right]. \quad (28)$$

We transform it to variables u, v which take values in $[0,1]$:

$$q = \exp[(M_1 + M_2)u - M_1], \quad k = \exp[(M_1 + M_2)v - M_1], \quad (29)$$

where q, k are in GeV/c and $M_{1(2)}$ is a lower (upper) integration limit in $\ln k$. Then (28) goes into

$$H\phi(u) = -2(M_1 + M_2)\int_0^1 dv \left[\frac{\phi(v) - f(u-v)\phi(u)}{|f(u-v) - 1|} + \frac{\phi(u)}{\sqrt{1 + 4f^{-2}(u-v)}}\right], \quad (30)$$

where

$$f(u) = \exp[(M_1 + M_2)u]. \quad (31)$$

Now we discretize the interval [0,1] in u and v into n equidistant points $u_0, u_1, \cdots, u_n$ and $v_0, v_1, \cdots, v_n$ to convert the evolution equation (26) into a set of n ordinary 1st order non-linear differential equations in y. This set of equations can be solved by standard methods. We used the simplest 2nd order Runge–Kutta algorithm. The standard values of n and of the number of iterations to evolve in two units of $\tilde{y}$ were 800. We have studied the evolution of $\phi(y,q)$ from the initial value at $y = 0$ up to $\tilde{y} = 10$. The (fixed) value of the strong coupling $\alpha_s = g^2/4\pi$ has been chosen to be 0.2. With this choice our maximal rapidity is around 50.

An evident difficulty which one meets are the values of $H\phi$ at endpoints u_0 and u_n, at which the introduced cutoffs make the results unreliable. To overcome this difficulty we calculated $H\phi$ at these points by extrapolation from the neighbouring points. The stability of this procedure was checked by comparing the results for double and quadruple values of n.

The initial function is determined by the color density of the nucleon $\rho_N(r)$ according to (27). To simplify our calculations we have taken the Yukawa form for $\rho_N(r)$:

$$\rho_N(r) = \frac{\mu}{2\pi}\frac{e^{-\mu r}}{r}, \quad (32)$$

where $\mu = 1/0.7\,\text{fm}$ has the meaning of an inverse nucleon radius. This choice may look a bit arbitrary, but our results show that with growing rapidity the system quickly forgets not only the form but even the absolute magnitude of ρ_N, so that the solution becomes independent of the initial function and appears to be governed only by the internal dynamics of (26) itself.

Doing the integrations over r and r_1 in (27) and over ν inside the BFKL Green function (3) we find for $q > \mu$

$$\tilde{\phi}_0(q)_{q>\mu} = B\frac{\mu^2}{q^2} \times \left\{1 - \frac{\mu}{q\sqrt{\pi}}\sum_{n=0}(-1)^n\left(\frac{\mu^2}{q^2}\right)^n \frac{\Gamma(1/2+n)}{(n+3/2)^2}\right\} \quad (33)$$

and for $q < \mu$

$$\tilde{\phi}_0(q)_{q<\mu} = B\left\{\frac{1}{4}\left[\left(2\ln\frac{q}{\mu} + \psi(3/2) - \psi(1) - 1\right)^2 + \psi'(3/2) + \psi'(1) + 1\right] - \frac{q^2}{\sqrt{\pi}\mu^2}\sum_{n=0}(-1)^n \times \left(\frac{q^2}{\mu^2}\right)^n \frac{\Gamma(5/2+n)}{(n+2)(n+1)^3}\right\}, \quad (34)$$

where the dimensionless coefficient

$$B = \frac{g^4}{16\pi}\frac{AT(b)}{\mu^2} \quad (35)$$

carries all the information about the nucleus. Its maximal value with $\alpha_s = 0.2$ is about 0.12 for the central scattering on lead ($b = 0$). The asymptotic behavior of $\phi_0(q)$ at $q \to \infty$ and $q \to 0$ is governed by the first terms in (33) and (34), which come from the poles of the BFKL Green functions at $\nu = \pm i/2$:

$$\phi_0(q) \sim 1/q^2, \quad q \to \infty, \phi_0(q) \sim \log^2 q, \quad q \to 0. \quad (36)$$

We have checked that our results practically do not change if the complicated function which multiplies B in (33) and (38) is substituted just by $\ln^2(q/(\mu + q)$ with the same asymptotic behavior (36).

The initial function depends on the form of the nucleus profile function $T(b)$. For our numerical calculation we have chosen

$$T(b) = 2\sqrt{R_A^2 - b^2}/V_A \quad (37)$$

corresponding to a finite nucleus of radius R_A and volume V_A with a constant density. We have taken $R_A = A^{1/3}R_0$ with $R_0 = 1.2\,\mathrm{fm}$.

Our results for $\phi(q)$ for two values of $B = 0.12$ and 0.02, corresponding to a central and very peripheral collisions off lead, respectively, are presented in Figs. 2 and 3. One observes that the solution ϕ at rapidities $\tilde{y} > 2$ evolves to a very simple and universal form, practically independent of the initial function. Crudely speaking it linearly falls with $\xi = \ln k$ until it meets the x-axis; from where it does it stays equal to zero. The slope of the falling part is exactly equal to 1, so that very crudely

$$\begin{aligned} &\phi(\xi) = \xi_1(y,b) - \xi, \quad \text{for} \quad \xi < \xi_1(y,b), \\ &\phi(\xi) = 0, \quad \text{for} \quad \xi > \xi_1(y,b). \end{aligned} \quad (38)$$

The value of $\xi_1(y,b)$ and hence the interception point with the x-axis grow linearly with y, so that with the growth of y the picture simply shifts to the right. In reality the curve for ϕ of course has no break: the two straight lines of which it is formed join smoothly in the vicinity of ξ_1. As will become clear later, the physically important region is precisely this vicinity, where ϕ is not trivial.

The results for $\phi(k)$ do not depend on the chosen cutoffs, provided they are taken to cover the region around the interception point ξ_1. Otherwise the evolution stops as soon as ξ_1 touches the upper cutoff M_2. So if one wants to study evolution up to high values of y the upper cutoff should be taken correspondingly high. In our calculations we chose $M_1 = 10$ and $M_2 = 30$, having verified that further raising of either M_1 or M_2 does not change the results.

In conclusion we find that ϕ does not possess any finite limit as $y \to \infty$ so that (26) does not lead to any saturation of the wave function ϕ at high rapidities, contrary to naive expectations. However, in the next chapter we shall see that such a saturation indeed occurs for physical quantities. The point is that the function ϕ by itself has no physical meaning. It is its derivatives which matter.

4 Nuclear structure function and the gluon density

The nuclear structure function is obtained in the standard manner as

$$F_2(x,Q^2) = \frac{Q^2}{\pi e^2}(\sigma_\mathrm{T} + \sigma_\mathrm{L}), \quad (39)$$

where the $\sigma_{\mathrm{T,L}}$ are the total cross-section for the scattering on the nucleus of a virtual photon with transversal (T) or longidunal (L) polarization. Both cross-sections can be found from the imaginary part of the forward scattering amplitude (10). In terms of $\tilde{\phi}$ we find

$$\sigma_{\mathrm{T,L}} = 4\pi \int \mathrm{d}^2b\mathrm{d}^2r\rho_{\mathrm{T,L}}(r)r^2\tilde{\phi}(y,r,b). \quad (40)$$

Here we explicitly indicated the dependence of ϕ on the impact parameter; the $\rho_{\mathrm{T,L}}(r)$ are the well-known color densities of the virtual photon split into a $q\bar{q}$ pair (see e.g. [15]). With massless quarks

$$\rho_T(r) = \frac{e^2N_cZ^2}{8\pi^3}\int_0^1 \mathrm{d}\alpha(\alpha^2 + (1-\alpha)^2)\epsilon^2\mathrm{K}_1^2(\epsilon r) \quad (41)$$

and

$$\rho_\mathrm{L}(r) = \frac{e^2N_cZ^2}{2\pi^3}Q^2\int_0^1 \mathrm{d}\alpha\alpha^2(1-\alpha)^2\mathrm{K}_0^2(\epsilon r), \quad (42)$$

where $\epsilon^2 = Q^2\alpha(1-\alpha)$ and Z^2 is a sum of squares of quark electric charges in units e.

Passing to momentum space we find

$$\sigma_{\mathrm{T,L}} = 4\pi \int \mathrm{d}^2b\frac{\mathrm{d}^2q}{(2\pi)^2}\tilde{\phi}(q,y,b)w_{\mathrm{T,L}}(q), \quad (43)$$

where

$$w_{\mathrm{T,L}}(q) = \int \mathrm{d}^2r r^2\rho_{\mathrm{T,L}}(r)\mathrm{e}^{\mathrm{i}qr}. \quad (44)$$

A straightforward calculation leads to the following expressions for $w_{\mathrm{T,L}}(q)$. For the transverse density one finds[1]

$$\begin{aligned} w_T(q) = \frac{e^2N_cZ^2}{8\pi^2}\int_0^1 \mathrm{d}\alpha(\alpha^2 + (1-\alpha)^2) \\ \times \nabla_q^2[(q^2/2 + \epsilon^2)J(q,\epsilon)], \end{aligned} \quad (45)$$

where

$$J(q,\epsilon) = \frac{2}{q\sqrt{q^2+4\epsilon^2}}\ln\frac{\sqrt{q^2+4\epsilon^2}+q}{\sqrt{q^2+4\epsilon^2}-q}. \quad (46)$$

The longitudinal density w_L is given by the same expression with the substitutions

$$\alpha^2 + (1-\alpha)^2 \to \alpha(1-\alpha), \quad q^2/2 + \epsilon^2 \to -4\epsilon^2.$$

[1] An error in this formula led to some erroneous conclusions about the y behavior of the structure function in the original version

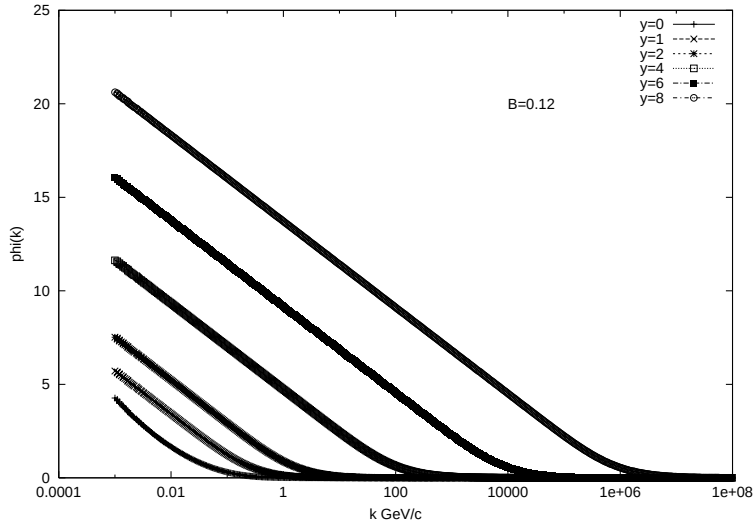

Fig. 2. ϕ as a function of momentum at different y (in units $\pi/\alpha_{\rm s}N$) for central collisions on lead ($B = 0.12$, (359))

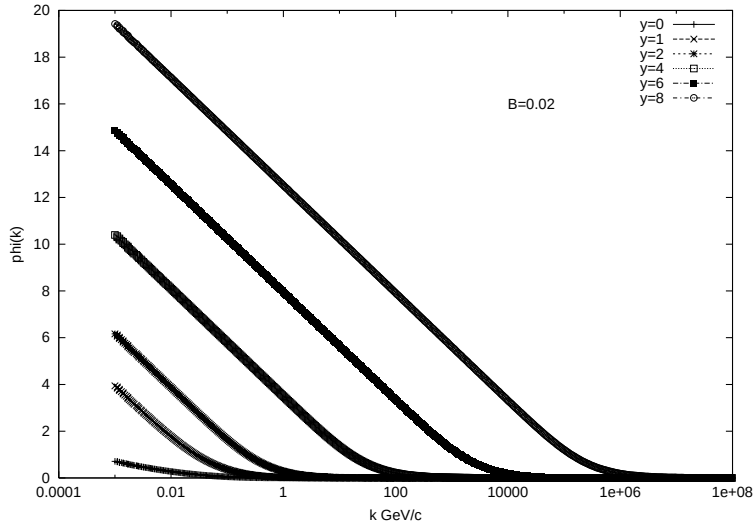

Fig. 3. ϕ as a function of momentum at different y (in units $\pi/\alpha_{\rm s}N$) for peripheral collisions on lead ($B = 0.02$, Eq.(35))

With the numerical values found for the function ϕ in the range $0 \le \tilde{y} \le 10$ we evaluated the nuclear structure function of lead ($A = 207$) for various values of Q^2 between 3 and $10^5\,(\mathrm{GeV}/c)^2$. The results are most instructive for the cross-section $\sigma_{\rm L}$ for the scattering of a longitudinally polarized virtual photon on the nucleus. In Figs. 4 and 5 we present it (with $e^2 \to 1$) as a function of y at fixed Q^2 and as a function of Q^2 at fixed y respectively (in GeV^{-2}). From Fig. 4 one clearly sees saturation in rapidity: for any value of Q^2 the cross-section tends to the same limit of $228.8\,(\mathrm{GeV}/c)^{-2} = 0.1768R_A^2$ as $\tilde{y}$ goes beyond 5. The resulting constant cross-section is evidently consistent with the unitarity restrictions. In terms of the complex angular momentum j our results indicate that the original cut at $j > 1$ is reduced to a simple pole at $j = 1$. Figure 5 illustrates the unusual behavior in Q^2 which sets in at high y: instead of going down as $1/Q$ in the standard BFKL approach, the cross-section becomes independent of Q^2 to a very high precision.

These results for the longitudinal cross-section can be conveniently interpreted in terms of scattering of color dipoles off the nucleus. The density $\rho_{\rm L}(r)$, appropriately normalized, can be interpreted as a probability distribution for the longitudinal photon to split into color dipoles of transverse dimension r. The normalization factor

$$D = \int \mathrm{d}^2 r \rho_{\rm L}(r) = \frac{e^2 N_c Z^2}{12\pi^2} = 0.028145 e^2$$

can be considered as the total probability for the photon to split into dipoles. Then the dipole–nucleus cross-section is found by dividing $\sigma_{\rm L}$ by the factor D, which gives $8131.1\,(\mathrm{GeV}/c)^{-2}$, independent of Q^2, that is, of the dipole dimension. This value exactly equals $2\pi R_A^2$, corresponding to scattering off a black disk.

The transverse part of the structure function does not admit this interpretation, due to the fact that $\rho_{\rm T}(r)$ is not normalizable. As a result both the cross-section and the structure function do not saturate at large y but continue to grow nearly linearly in y. This is illustrated in Figs. 6 and 7 where the total structure function (including the much smaller longitudinal part) is shown as a function of $x = \mathrm{e}^{-y}$ and Q^2, respectively.

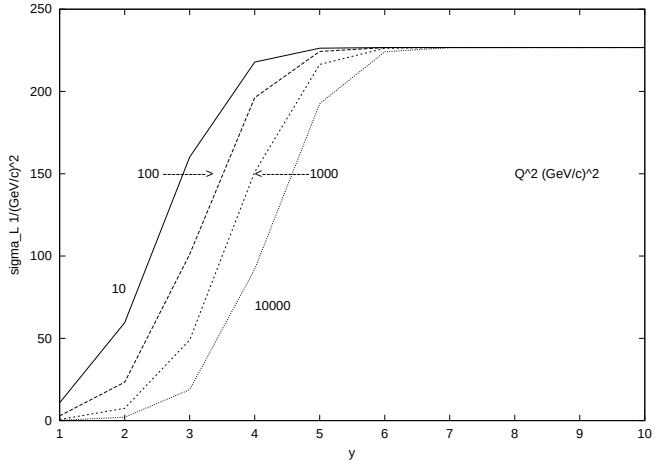

Fig. 4. Cross-section $\sigma_{\rm L}$ (with $\mathrm{e}^2 \to 1$) as a function of y (in units $\pi/\alpha_{\rm s}N$) for different Q^2

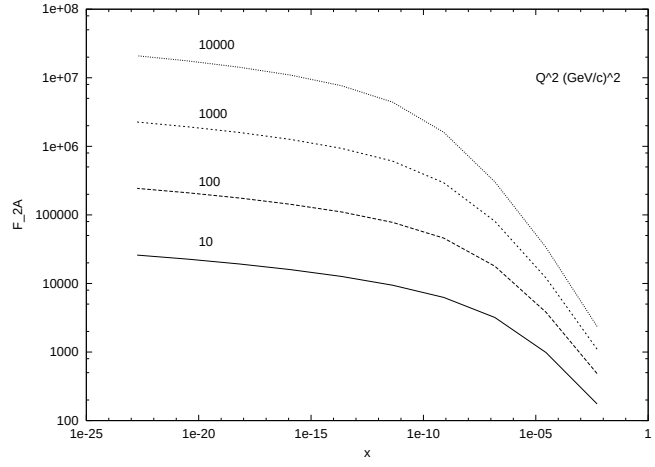

Fig. 6. The structure function of lead $F_{2A}(x, Q^2)$ as a function of x for different Q^2

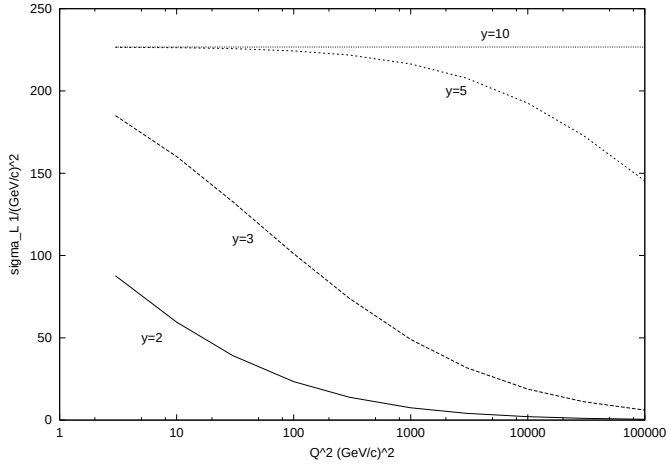

Fig. 5. Cross-section $\sigma_{\rm L}$ (with $e^2 \to 1$) as a function of Q^2 for different y (in units $\pi/\alpha_{\rm s}N$)

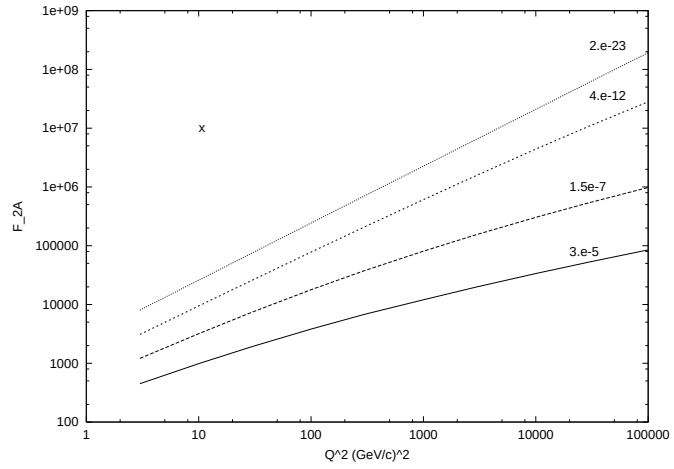

Fig. 7. The structure function of lead $F_{2A}(x, Q^2)$ as a function of Q^2 for different x

We finally come to the gluon density. Although strictly speaking it is not a physical quantity, its properties have been much discussed recently in connection with its saturation for a large nucleus [16]. It can be related to our function ϕ via the standard expression for the structure function in its terms (see e.g [14])

$$F_2(x, Q^2) = \frac{g^2 Q^2}{\pi^3 N e^2} \int \mathrm{d}^2 b \mathrm{d}^2 r [\rho_T(r) + \rho_L(r)] F(x, r, b), \tag{47}$$

where

$$F(x, r, b) = \int \frac{\mathrm{d}^2 k}{(2\pi)^2 k^4} k^2 \times \frac{\partial x G(x, k^2, b)}{\partial k^2} \left(1 - \mathrm{e}^{-\mathrm{i}kr}\right) \left(1 - \mathrm{e}^{\mathrm{i}kr}\right), \tag{48}$$

and $\int \mathrm{d}^2 b (\partial x G(x, k^2, b)/\partial k^2)$ is up to a factor the gluon density in the momentum space:

$$\frac{\partial N(l)}{\partial^2 l} = \frac{1}{\pi} \frac{\partial N(l)}{\partial l^2} = \frac{1}{\pi} \int \mathrm{d}^2 b \frac{\partial x G(x, l^2, b)}{\partial l^2}. \tag{49}$$

In the following we shall study the double density in momentum and impact parameter, which is just $\partial x G(x, k^2, b)/\partial k^2$. Comparing (47), (48) with the corresponding expression in terms of ϕ, which follows from (39) and (40) we find a relation

$$F(x, r, b) = \frac{4N}{\pi g^2} r^2 \tilde{\phi} \left(\ln \frac{1}{x}, r, b \right). \tag{50}$$

Taking a Fourier transform of (48) and neglecting the term proportional to $\delta^2(k)$ we obtain

$$\frac{\partial x G(x, k^2, b)}{\partial k^2} = \frac{2N}{\pi g^2} k^2 \nabla_k^2 \tilde{\phi} \left(\ln \frac{1}{x}, k, b \right). \tag{51}$$

This is the desired relation between our function ϕ and the gluon density in the combined momentum and impact parameter space.

Applying $k^2 \nabla_k^2$ to the function ϕ we thus find the gluon density up to a trivial numerical factor as is evident from (51)(~ 0.76 with $\alpha_{\rm s} = 0.2$). The function $h(k) =$

$k^2\nabla_k^2\tilde{\phi}(y,k,b)$ for different values of y and $B = 0.12$ and 0.02 is shown in Figs. 8 and 9. Its form at different y turns out to be quite remarkable. As one observes, at any given rapidity the found density has the same roughly Gaussian in shape in the variable $\xi = \ln k$, centered at the point $\xi = \xi_0(y)$ very near to ξ_1 at which the straight line (38) crosses the x-axis (see Sect. 2). With the growth of y the distribution moves to the right with a nearly constant velocity practically preserving its form. Approximately the distribution can be described by

$$h(k) = h_0 \mathrm{e}^{-a(\xi-\xi_0(y))^2}, \tag{52}$$

where h_0 and a are practically independent of y and $\xi_0(y)$ linearly grows with it:

$$h_0 \simeq 0.3, \quad a \simeq 0.3 \quad \xi_0(y) = \xi_{00} + 2.23\tilde{y}. \tag{53}$$

The only quantity which clearly depends on the initial distribution is the starting position ξ_{00}, so that for different initial functions the picture in Figs. 8 and 9 shifts along the ξ-axis as a whole.

Evidently at a given value of k the density stays always limited, irrespective of the form of the initial distribution (and of the atomic number A, in particular). In this sense we have saturation as discussed in [16]. However with the growth of y the strongly peaked density moves away toward higher values of k so that the density at a fixed point tends to zero at high values of rapidity. We thus have "supersaturation": with $y \to \infty$ the gluon density at an arbitrary finite momentum tends to zero.

Comparing Figs. 8 and 9 one can see how the memory about the initial distribution (except for ξ_{00}) is gradually erased in the course of the evolution in y. For a very peripheric collison off lead ($B = 0.02$) at the initial stages of the evolution the density is correspondingly much smaller than for a central collision ($B = 0.12$). However, already at $\tilde{y} = 2$ the form of the distribution is practically indistinguishable from the central collision, the only remaining difference being the shift along the ξ-axis.

5 Conclusions

The BFKL fan diagram equation has been solved numerically in the large range of rapidities up to $y = 50$. The main results are the following.

The idea that the fan diagrams themselves satisfy the unitarity condition has been supported by the fact that the cross-sections found for the scattering of a $q\bar{q}$ pair off the nucleus tend to a constant value at high rapidities. Since the found cross-sections do not increase with energy, the leading j plane singularity turns out to be a simple pole at $j = 1$. The limiting cross-sections prove to be universal: they do not depend on Q^2, that is, on the transverse dimension of the $q\bar{q}$ pair, nor on the initial color distribution inside the nucleon. Their dependence on the target nucleus thus reduces to a scale factor R_A^2. Physically they correspond to scattering of a color dipole off a black disk.

The nuclear structure function does not saturate at high rapidities, due to the singularity of the transverse distribution $\rho_{\mathrm{T}}(r)$ at $r = 0$, which makes it non-normalizable. At large y it continues to grow nearly linearly in y.

These results fully agree with predictions made in [11] on the basis of the found perturbative solution of the BFKL fan diagram equation and asymptotic estimates made in [12].

A completely novel result concerns the gluon density of the nucleus. At sufficiently high rapidities, greater than 10, the gluon density acquires a form of the soliton wave in y–$\ln k$ space, which, with the growth of y, moves along the $\ln k$ towards greater k preserving its nearly Gaussian shape. Thus at any finite k the gluon density eventually goes to zero at high enough k

Finally, we have to stress that all these properties begin to be clearly visible only at very high rapidities and momenta: $y > 10$ and $k > 100\,\mathrm{GeV}/c$ with $\alpha_{\mathrm{s}} = 0.2$. With smaller αs these values grow correspondingly.

Acknowledgements. The author is grateful to Dr. G.P. Vacca who drew his attention to the possibility to simplify the BFKL fan diagram equation. He is also grateful to Prof. Bo Andersson for his interest in this work and stimulating discussions. He thanks the Department for Theoretical Physics of the Lund University for hospitality during his stay in Lund, where this work was completed. The author is finally most thankful to Dr. Yu. Kovchegov, fruitful discussions with whom helped to find and correct an error in the expression for w_T ((45)) in the first version of this paper.

Appendix
Color dipole approach

To compare our BFKL fan diagram equation to that of Kovchegov [10] we present here a short derivation of (1) from the color dipole approach, which will make clear the difference between the two equations.

In the color dipole approach the single scattering term (2) can be presented in the form

$$\mathcal{A}(y,b) = -2\mathrm{i}sAT(b)\int \mathrm{d}^2r\rho(r)\int \mathrm{d}^2r_1 n_1(r,r_1,y)\tau(r_1), \tag{54}$$

where

$$\tau(r_1) = -\frac{1}{2}g^4\int \mathrm{d}^2r' G(0,r_1,r')\rho_N(r') \tag{55}$$

and $n_1(r,r_1,y)$ is the single dipole density at rapidity y introduced by Mueller; r_1 and r are the dipole lengths at rapidity y and at $y = 0$ respectively, so that

$$n_1(r,r_1,y)_{y=0} = \delta^2(r-r_1). \tag{56}$$

(Note that as in [10] our n_1 is Mueller's one divided by $2\pi r_1^2$.)

To introduce the multidipole densities Muller constructed a generating functional $Z(r_1,r_0,y|u)$, where

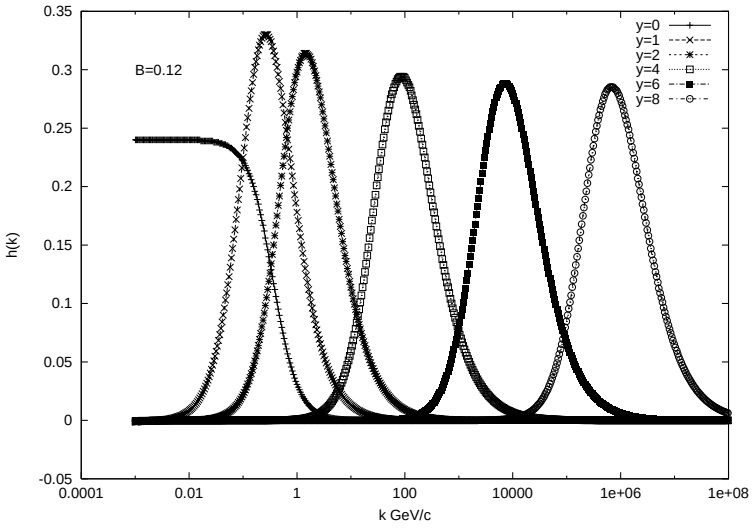

Fig. 8. The gluon density (in units $\pi^2 N/2\alpha_s$) as a function of momentum at different rapidities $\tilde{y}$ for central collisions on lead ($B = 0.12$, (35))

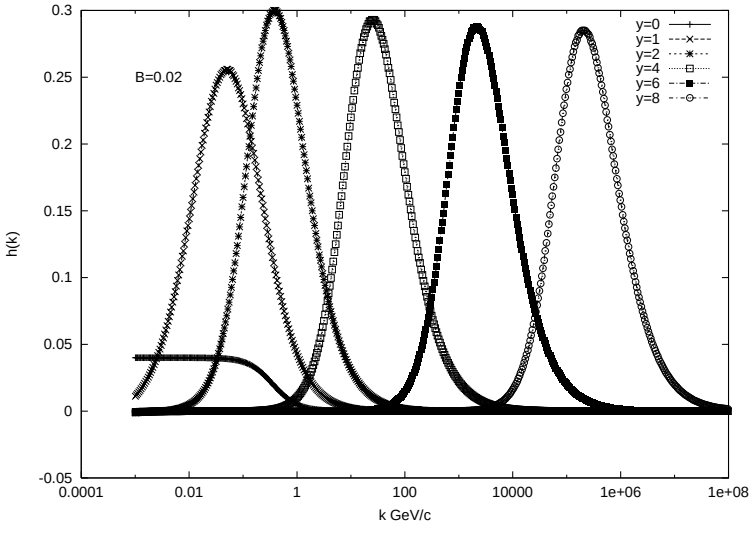

Fig. 9. The gluon density (in units $\pi^2 N/2\alpha_s$) as a function of momentum at different rapidities $\tilde{y}$ for peripheral collisions on lead ($B = 0.02$, (35))

$u = u(\rho_i, \rho_f)$ is a function of the two dipole endpoints in the transverse space (which, for brevity, we denote it by a single symbol ρ). The functional Z satisfies the following non-linear equation:

$$Z(r_1, r_2, y|u) = u(r_1, r_0)\mathrm{e}^{2y\omega(r_{10})} + \frac{g^2 N_c}{8\pi^3}\int_0^y \mathrm{d}y' \mathrm{e}^{2\omega(r_{10})(y-y')}\int \mathrm{d}^2 r_2 \times \frac{r_{10}^2}{r_{12}^2 r_{20}^2} Z(r_1, r_2, y'|u) Z(r_2, r_0, y'|u), \quad (57)$$

where $r_{10} = r_1 - r_0$ etc. and $\omega(r)$ is the gluon trajectory $\omega(q)$ in which the momentum q is substituted by r:

$$\omega(r) = -\frac{g^2 N_c}{4\pi^3}\ln\frac{r}{\epsilon} \quad (58)$$

with ϵ the cutoff at small r (in the ultraviolet). The functional Z is normalized according to

$$Z(r_1, r_0, y|u)_{u=1} = 1. \quad (59)$$

The k-fold inclusive dipole density is given by a k-fold derivative of D with respect to u at $u = 1$:

$$n_k(r_1, r_0, y; \rho_1, \cdots, \rho_k) = \frac{1}{k!}\frac{\delta^k Z}{\delta u(\rho_1), \cdots, \delta u(\rho_k)}_{u=1}. \quad (60)$$

At this point we make our first comment as to the comparison with [10]. Our form of the functional equation for Z is the same as in the original pater of Mueller [1] and in [10], except for a slightly different choice of dipole coordinates and for the order of arguments in the 2nd Z in the non-linear term: their form would correspond to $Z(r_0, r_2, y'|u)$. Comparing with the BFKL equation for the single dipole density, one can verify that our choice is better. However, this point is irrelevant for the following, since in the interaction with the nucleus only even functions of r_{10} appear.

The dipoles are to interact with the nucleus target with a zero transferred momentum. If the dimension of the dipole is smaller than the internucleon distance in the nucleus, then it will interact with a single nucleon as a whole. This picture lies at the basis of the standard fan

diagram approach, where each pomeron finally interacts with a single nucleon. We used precisely this picture in our derivation of (26) in Sect. 2. In this picture the only trace of the nucleus will be an additional factor $AT(b)$ multiplying the interaction with the nucleon $\tau(r)$ ((54)) at a given impact parameter b. In [10] a different idea is exploited: it is assumed that each of the dipoles can interact with many nucleons. The latter interaction is assumed to have an eikonal form. So the interaction with the nucleus they consider is a two-stage one: first the projectile generates many color dipoles (BFKL fan diagrams) and then each dipole multiply interacts with the nucleus à la Glauber. Although technically it is not difficult to take into account the final eikonalization of the interaction, appropriately changing the single scattering term $\tau(r)$ in (55) and the following formulas, we do not think it is reasonable. On the one hand, as we shall see, in the interaction with the nucleus the densities are considerably damped at large distances as compared to the usual BFKL behavior. The confinement should further restrict their spatial dimensions. So for a nucleus with a large internucleon distance it does not seem reasonable to assume simultaneous interaction of a dipole with two or more nucleons. On the other hand, should such interactions be really important, one cannot expect to correctly describe the interaction with the nucleus of a dipole of a given (and fixed) dimension by the Glauber formula. Note that the expression used in [9] does not correspond to the BFKL picture for the scattering on a single nucleon. So we take τ as given by (55) and this is the main difference between our derivation and that of [10].

With a chosen τ, the interaction with the nucleus will be described by densities

$$\nu_k(r_1, r_0, y) = \int \prod_{j=1}^{k} (\mathrm{d}^4\rho_j \tau(\rho_j) AT(b)) \times n_k(r_1, r_0, y; \rho_1, \cdots, \rho_k). \tag{61}$$

Here $\tau(\rho) = \tau(\rho_f - \rho_i)$ depends only on the dipole length and is given by (55).

Differentiating (57) and using (61) one easily obtains

$$\nu_1(r_1, r_0, y) = AT(b)\tau(r_{10})\mathrm{e}^{2y\omega(r_{10})} + \frac{g^2 N_c}{8\pi^3} \int_0^y \mathrm{d}y' \mathrm{e}^{2\omega(r_{10})(y-y')} \int \mathrm{d}^2 r_2 \times \frac{r_{10}^2}{r_{12}^2 r_{20}^2} [\nu_1(r_1, r_2, y') + \nu_1(r_2, r_0, y')] \tag{62}$$

and for $k > 1$

$$\nu_k(r_1, r_0, y) = \frac{g^2 N_c}{8\pi^3} \int_0^y \mathrm{d}y' \mathrm{e}^{2\omega(r_{10})(y-y')} \int \mathrm{d}^2 r_2 \frac{r_{10}^2}{r_{12}^2 r_{20}^2} \times \left[[\nu_k(r_1, r_2, y') + \nu_k(r_2, r_0, y') + \sum_{j=1}^{k-1} \nu_j(r_1, r_2, y') \nu_{k-j}(r_2, r_0, y') \right]. \tag{63}$$

We suppress the evident dependence on the impact parameter b.

From the structure of the equations and the form of the inhomogeneous term it follows that the densities $\nu(r_1, r_0, y)$ depend only on the initial dipole length r_{10}. As a result, the two terms separated from the sum over j on the right-hand side give the same contribution. One then finally finds the equations

$$\nu_1(r_{10}, y) = AT(b)\tau(r_{10})\mathrm{e}^{2y\omega(r_{10})} + \frac{g^2 N_c}{4\pi^3} \int_0^y \mathrm{d}y' \mathrm{e}^{2\omega(r_{10})(y-y')} \times \int \mathrm{d}^2 r_2 \frac{r_{10}^2}{r_{12}^2 r_{20}^2} \nu_1(r_{20}, y'), \tag{64}$$

and for $k > 1$

$$\nu_k(r_{10}, y) = \frac{g^2 N_c}{4\pi^3} \times \int_0^y \mathrm{d}y' \mathrm{e}^{2\omega(r_{10})(y-y')} \int \mathrm{d}^2 r_2 \frac{r_{10}^2}{r_{12}^2 r_{20}^2} \nu_k(r_{20}, y') + \frac{g^2 N_c}{8\pi^3} \int_0^y \mathrm{d}y' \mathrm{e}^{2\omega(r_{10})(y-y')} \times \int \mathrm{d}^2 r_2 \frac{r_{10}^2}{r_{12}^2 r_{20}^2} \sum_{j=1}^{k-1} \nu_j(r_{12}, y') \nu_{k-j}(r_{20}, y'). \tag{65}$$

The total forward scattering amplitude on the nucleus will be given by the expression (54) in which the single dipole interaction $\int \mathrm{d}^2 r_1 n_1(r, r_1, y) \tau(r_1)$ is substituted by the sum of all multidipole interactions $\sum_k \nu_k(r)$. Presenting the amplitude in the form (10) we have

$$\Phi(r, y) = -\sum_{k=1} \nu_k(r, y). \tag{66}$$

Summing (64) and (65) over k we obtain an equation for Φ:

$$\Phi(r_{10}, y) = -AT(b)\tau(r_{10})\mathrm{e}^{2y\omega(r_{10})} + \frac{g^2 N_c}{4\pi^3} \times \int_0^y \mathrm{d}y' \mathrm{e}^{2\omega(r_{10})(y-y')} \int \mathrm{d}^2 r_2 \frac{r_{10}^2}{r_{12}^2 r_{20}^2} \Phi(r_{20}, y') - \frac{g^2 N_c}{8\pi^3} \int_0^y \mathrm{d}y' \mathrm{e}^{2\omega(r_{10})(y-y')} \int \mathrm{d}^2 r_2 \frac{r_{10}^2}{r_{12}^2 r_{20}^2} \times \Phi(r_{12}, y') \Phi(r_{20}, y'). \tag{67}$$

Comparing this equation with the one derived in [10], apart from a different inhomogeneous term, which was discussed earlier, we find a difference in the spatial arguments of the function Φ. Our Φ depends only on one such argument: the dipole dimension r_{12}. The equivalent Kovhegov function N depends on two spatial arguments: it depends not only on the dipole dimension but also on its center-of-mass coordinate b_0, not to be confused with the impact parameter b which does not enter his equation at all. The dependence on b_0 should be governed by the inhomogeneous term, which seems to be independent of b_0 ((6a) of [10]). Then the dependence of N on the 2nd argument seems to disappear and Kovchegov's equation

coincides with (67). However, this contradicts his initial formula ((4) of [10]) in which one integrates over all b_0. Modulo all these (small) inconsistencies and a different inhomogeneous term, our (67) coincides with Kovchegov's.

References

1. A. Mueller, Nucl. Phys., B **415**, 373 (1994)
2. A. Mueller, B. Patel, Nucl. Phys., B **425**, 471 (1994)
3. M.A. Braun, G.P. Vacca, Eur. Phys. J C **6**, 147 (1999)
4. R. Peschanski, Phys. Lett. B **409**, 491 (1997)
5. A. Schwimmer, Nucl. Phys. B **94**, 445 (1975)
6. L.V. Gribov, E.M. Levin, M.G. Ryskin, Nucl. Phys. **188**, 555 (1981); Phys. Rep. **100**, 1 (1983)
7. J. Bartels, M. Wuesthoff, Z. Phys., C **66**, 157 (1995)
8. M.A. Braun, Eur. Phys. J C **6**, 321 (1999)
9. I. Balitsky, hep-ph/9706411; Nucl. Phys. B 463 (1996) 99
10. Yu. Kovchegov, Phys. Rev D **60**, 034008 (1999)
11. Yu. Kovchegov, preprint CERN-TH/99-166 (hep-ph/9905214)
12. E. Levin, K. Tuchin, preprint DESY 99-108, TAUP 2592-99 (hep-ph/9908317)
13. L.N. Lipatov in: Perturbative QCD, edited by A.H. Mueller (World Scientific, Singapore 1989) p. 411
14. M.A. Braun, Eur. Phys. J C **6**, 343 (1999)
15. N.N. Nikolaev, B.V. Zakharov, Z. Phys. C **64**, 631 (1994)
16. A. Mueller hep-ph/9904404; 9906322; 9902302